Scaling of impact on low fibre-volume glass–polyester laminates

L. S. Sutherland and C. Guedes Soares

Abstract

A dimensional analysis approach has been used to develop scaling laws for impact on marine composite materials. An experimental study has been carried out to verify these relationships for the transverse impact of a hemispherical ended impactor on fully clamped circular hand laid-up glass–polyester plates at three different scales. Although the model was a simplified one, the tests showed that it scaled the impact responses well for the elastic response. However, some 'size effects' were observed, especially for the damaged response, and further work is required to fully explain the mechanisms behind these effects.

Keywords

Scaling, A. Glass fibres, A. Thermosetting resin, B. Impact behaviour

1. Introduction

The fact that composite materials are susceptible to damage due to impact events is well known, and the problem has received a great deal of attention in the literature [1]. The case of a central transverse impact on a laminated plate by a relatively small, usually hemispherical ended, steel impactor is most often studied as a severe event. The great majority of the literature concerns high fibre volume-fraction, pre-preg carbon–epoxy autoclaved laminates as used in the aerospace industry. The current work, however, concerns much more variable hand laid-up lower priced, low fibre-content glass–polyester composites as commonly used in the marine industry.

Impact on composites is a complex problem largely due to the following points.

- Large deflections and shear deflections and membrane effects are usually significant.
- Local forces under the impactor give non-linear contact behaviour.
- Impact is a dynamic event.
- Damage modes are numerous and interacting, including internal delamination, surface micro buckling, fibre fracture and matrix degradation.
- The response and damage modes are sensitive not only to the exact nature of the composite, but also to the many impact parameters.

Hence, confidence in theoretical predictions is not high, especially concerning damage, and so experimental validation of the design process is often necessary. Full-scale testing may not be feasible, and is certainly expensive, and hence scale model testing is attractive.

However, there are scaling issues; it is necessary to be certain that there are no unforeseen phenomena or differences in behaviour that lead to errors in full-scale prototype predictions obtained from model tests. Such prediction errors are referred to as 'size-' or 'scale-effects'. Considerable work has also been carried out in the area of size-effects in composites testing, with a general consensus that these effects are significant, but that there is no one single phenomenon because of the various failure mechanisms involved [2].

Work specifically concerning the scaling of the impact on composites is much scarcer, however. Morton and Pintado [3,4] applied dimensional analysis techniques to ensure completely similar pre-preg carbon–epoxy model and prototype beams. Elastic behaviour was successfully scaled, but a damage size effect was significant – smaller specimens were stronger. Weakest link theory and fracture mechanics [5] were suggested as possible mechanisms.

Swanson and co-workers [6–9] applied dimensional analysis to the dynamic plate response differential equations to arrive at the same scaling laws. The undamaged behaviour of carbon–epoxy pre-preg plates and filament wound cylinders also followed the scaling laws, but larger specimens suffered more damage and were weaker. No mechanism for these scale effects was concluded. Sankar [10] used a similar technique to Swanson, limited to a numerical parametric study for cases without damage.

Ambur et al. [11] extended the scaling laws to include non-linear effects with success for the elastic response of graphite–epoxy pre-preg laminates, but again more damage was observed at the larger scale. The magnitude of this damage size effect was different for ply level and sub-ply level scaling.

A study of the scaling of quasi-static transverse loading of carbon–epoxy pre-pregs by Nettles et al. [12] again showed that elastic responses scaled well, but that smaller specimens were stronger and that larger specimens suffered larger damage areas. Also, dent depths did not scale well, and variability was higher at smaller scale.

Drop tests on 1/5- and full-scale fuselage sections were performed by Jackson et al. [13]. Average accelerations were between 4% and 15% lower for the model. Practical scaling problems especially resin content (and hence mass) and suspension mountings were thought to be important.

Found et al. [14] and Liu et al. [15] scaled woven and unidirectional carbon–epoxy laminates respectively. Since geometrically distorted models were used, it was difficult to make scaling comparisons or conclusions.

A slightly different approach is not to try to ensure similarity, but to use distorted models and then use a complete knowledge of the system behaviour to ‘correct’ for these distortions. This is a daunting prospect considering the complexity of the impact event, especially when damage is present, but some authors have been successful using finite element methods.

Davies and co-workers [16–18] used an FE analysis (including non-linear contact, shear deformations, membrane effects and fibre damage) to scale the impact response of carbon–epoxy laminates. Force-damage area plots for coupon tests were used to verify the FE results at the larger scale. The onset of delamination was scaled using a fracture mechanics approach. However, for glass–polyester laminates the method was not successful and an empirical scaling rule was developed.

Linear and non-linear FE analyses were applied by Kistler and Waas [19] to graphite–epoxy cylindrical shells. Damage was not considered. Scaling by either momentum or kinetic energy was successful, depending on which input parameter was kept constant and whether deflections were large or small.

Few have studied the scaling of impact on sandwich laminates, and most of this work concentrates on the impact tolerance. Tomblin et al. [20] considered carbon–epoxy Nomex cored panels, validating an FE model with experimental work. Compression after impact (CAI) tests showed that the impact resistance (i.e., damage) must scale properly if impact tolerance is also to scale. Moody et al. [21] tested similar sandwich laminates, as well as curved panels, with similar conclusions. Zenkert et al. [22] did not consider the impact event itself; instead the damage tolerance was scaled to develop an inspection-based approach. A progressive micro-buckling analysis was successfully applied to the delamination and crack damage of carbon–vinylester PVC foam panels for CAI and hydrostatic pressure loading.

An FE analysis of single-skin graphite–epoxy coupons and stiffened panels by Chen et al. [23] concluded that damage scaling effects and not stress redistribution is the main cause of the damage tolerance scaling effect.

In summary, the use of scaling laws has been successful for the elastic response of high volume-fraction pre-preg carbon laminates, but damage size-effects were significant. The aim of the present work is to investigate experimentally the impact scaling of low fibre-volume hand-produced glass–polyester laminates using a scaled model approach.

2. Scaling theory

In this section scaling rules for the central, transverse impact of a fully clamped composite plate with a hemispherical ended impactor 'head' are developed using dimensional analysis techniques, the theory of models and also the system equation approach [24–26,11].

Firstly it is necessary to decide which response we wish to scale. In this paper this *test variable* will be the central displacement, $w(t)$. In order to simplify what is an extremely complex event, the impact behaviour of the composite is assumed to be sufficiently approximated by that of a homogenous and isotropic material.

Making a list of all of the variables thought to be relevant:

Specimen thickness	h
Specimen Radius	R
Specimen Poisson Ratio	υ
Specimen Young's Modulus	E
Specimen Density	ρ
Impactor Head Radius	R_i
Impactor Mass	m_i
Impactor Poisson Ratio	υ_i
Impactor Young's Modulus	E_i
Impactor Density	ρ_i
Incident Velocity	V_i

Using mass (M), length (L) and time (T) as the primary quantities and applying the Buckingham Pi theorem gives the 10 required (i.e. 13 variables minus 3 primary quantities) Pi terms given below. This particular set is not the only possible one, but has been selected because most of the terms have fairly straightforward physical interpretations.

Test parameter: $\Pi_1 = w/h$ (1)

Design parameters:

'Geometric' $\Pi_2 = R/h$, $\Pi_3 = R_i/h$ (2)

'Material property' $\Pi_4 = \upsilon$, $\Pi_5 = \upsilon_i$, $\Pi_6 = \rho/\rho_i$, $\Pi_7 = E_i/E$ (3)

'Impact event' $\Pi_8 = V_i^2 \rho_i / E$, $\Pi_9 = m_i / h^3 \rho_i$, $\Pi_{10} = tV_i/h$ (4)

Now the model needs to be designed to ensure that the test parameter (Π_1) is the same for model and prototype. The theory of models shows that to do this it is necessary to scale all of the relevant variables between model and prototype so that all the design parameters ($\Pi_{2–10}$) are also the same for model and prototype. If this is achieved (and this is not always physically possible) then the model is said to show complete similarity to the prototype. Defining the scaling factor, λ, of a variable as the ratio of its value for the prototype to that for the model. For example, for displacement:

$$\lambda_w = w_p / w_m \quad (5)$$

where subscripts p and m refer to prototype and model respectively.

Hence, extending this definition to the Pi terms gives the following relationship for complete similarity:

$\lambda_\Pi = 1$ for all Π, (6)

where, if $\Pi = f(x_1 \ldots x_j)$, then $\lambda_\Pi = f(\lambda_{x1} \ldots \lambda_{xj})$.

Constructing a model that is a geometrically scaled version (by a scaling factor of *s*) of the prototype will ensure that both $\lambda_{\Pi 2}$ and $\lambda_{\Pi 3}$ are unity:

i.e. $\lambda_h = \lambda_R = \lambda_{Ri} = s$ (7)

Using the same materials for the model as for the prototype, and using the same material for the impactor in both cases, will ensure that all of the material property scaling parameter factors ($\lambda_{\Pi 4}$ to $\lambda_{\Pi 7}$) are also unity:

i.e. $\lambda_\nu = \lambda_{\nu i} = \lambda_\rho = \lambda_{\rho i} = \lambda_E = \lambda_{Ei} = 1$ (8)

Now it only remains to ensure that the impact event itself is properly scaled, and to do this the scaling factors of the remaining Pi terms must also be unity:

$\lambda_{\Pi 8} = \lambda_{Vi}^2 \lambda_{\rho i} / \lambda_E = 1$, i.e. $\lambda_{Vi} = 1$ (9)

That is, the impact velocity (and hence the drop height) should be the same at model and prototype scales.

$\lambda_{\Pi 9} = \lambda_{mi} / \lambda_h^3 \lambda_{\rho i} = 1$, i.e. $\lambda_{mi} = s^3$ (10)

That is, the prototype impact mass should be s^3 times that of the model.

$\lambda_{\Pi 10} = \lambda_t \lambda_{Vi} / \lambda_h = 1$, i.e. $\lambda_t = s$ (11)

Since it is not possible to scale time this means that something that takes 1 s in the model will take *s* seconds in the prototype.

In summary, when target and impactor head are geometrically scaled as *s*, the same materials are used for model and prototype throughout, and the impact mass is scaled as s^3 and dropped from the same drop height for model and prototype, then we have complete similarity and the central displacement response should also scaled geometrically as *s*.

i.e. $\lambda_w = w_p / w_m = s$ (12)

It was already noted that time is also scaled by *s*, so the impact duration of the prototype would be expected to be *s* times that of the model, and now we will consider how the other commonly used impact responses scale in our model. Adding the variable impact force, *P*, to the initial list and applying Buckingham Pi theory gives an additional Pi term:

$\Pi_{11} = P/h^2 E$, i.e. $\lambda_P = s^2$ (13)

That is, the prototype impact force will be s^2 times that in the model.

Similarly, for the absorbed energy, AE:

$\Pi_{12} = AE/h^3 E$, i.e. $\lambda_{AE} = s^3$ (14)

That is, the prototype absorbed energy will be s^3 times that in the model.

The same method could also be used for the incident energy, IE;

$\Pi_{13} = IE/h^3 E$, i.e. $\lambda_{IE} = s^3$ (15)

Or alternatively, since the relationship for incident energy is known, it is equally possible to use the system equation approach:

$IE = \frac{1}{2} m_i V_i^2$, and hence, $\lambda_{IE} = \lambda_{mi}\lambda_{Vi}^2 = s^3$ (16)

It should be noted that the scaling model used here is simplified. Many aspects, such as the non-homogeneous and non-isotropic nature of the composite materials, the effect of damage, contact stiffness and possible strain-rate effects (c.f. $\lambda_t = s$) have not been included in the analysis. If any of these aspects have a significant effect on one or more of the responses then the lack of this effect in this simple analysis could lead to a 'distorted model'. This would produce deviations from the predictions of the analysis, which are often termed 'size-' or 'scale-effects'.

Here, the scaling analysis of the central impact of a fully clamped composite plate described above is verified through an experimental study. A series of tests are carried out at the model scale (i.e., *s* = 1) and these results compared with equivalent tests at two larger prototype scales (*s* = 2, and *s* = 3).

3. Experimental details

One metre square panels of orthotropic polyester resin reinforced with E-glass were laminated by hand. Two series of panels were fabricated; one using a 500 gm^{-2} woven roving (WR) reinforcement and one using 450 gm^{-2} chopped strand mat (CSM). Fibre mass-fractions were 0.5 (volume fraction 0.35) and 0.3 (volume fraction 0.2) for WR and CSM laminates, respectively. Square specimens were cut from the panels using a diamond-surrounded circular saw, and thickness measurements taken at four points on each. As explained in Section 2, specimens were geometrically scaled, and details are given in Table 1.

	s	No. Plies	No. Tests	Thickness (mm) Ave. / COV*	Clamp ∅ (mm)	Impact Mass (kg)	Head ∅ (mm)	Filter (kHz)
WR	1	5	6	3.06 / 4.1% (6.1%)	100	3.103	10	2
Clamp ∅ / Thickness = 32	2	10	6	6.14 / 4.1% (4.8%)	200	24.92	20	1
	3	15	4	9.44 / 3.0% (4.8%)	300	84.22	30	0.6
WR	1	10	6	6.29 / 2.1% (3.4%)	100	3.103	10	4
Clamp ∅ / Thickness = 16	2	20	6	12.12 / 2.0% (3.4%)	200	24.92	20	2
	3	30	3	18.30 / 2.1% (2.9%)	300	84.22	30	1.3
CSM	1	5	5	4.63 / 2.4% (8.2%)	100	3.103	10	2
Clamp ∅ / Thickness = 22	2	10	5	8.84 / 3.2% (5.3%)	200	24.92	20	1
	3	15	4	14.36 / 4.8% (12.1%)	300	84.22	30	0.75
CSM	1	10	6	8.67 / 5.0% (6.7%)	100	3.103	10	4
Clamp ∅ / Thickness = 11	2	20	6	18.54 / 7.4% (9.9%)	200	24.92	20	2

*Coefficients of variation are between specimen thickness averages, (values in parenthesis are between all thickness measurements).

Table 1. Specimen and test details

A fully instrumented falling weight machine (Rosand IFW5) was used for the impact testing. A light, hemispherical-ended cylindrical 'impactor head' attached to a much larger, variable mass was dropped from a known, variable height between guide rails onto the target. As per Section 2, the impactor heads were also geometrically scaled and the impact mass scaled as s^3 (see Table 1).

The horizontally supported specimens were fully clamped between thick steel annular plates to give the scaled specimen diameters. The thickness of the different clamping plates was also scaled geometrically.

A load cell between the impact mass and head gave the variation of impact force with time. An optical gate measured the incident velocity, and hence the impacter displacement and velocity and the energy it imparts could be calculated from the force–time data by successive numerical integrations. A pneumatic catching device, triggered by the return through the optical gate, prevented further rebound impacts. This device was not robust enough to be used for the largest impact mass (s = 3), and that rebounds occurred for this largest scale should be noted when considering the damage sustained by these specimens. However, the corresponding impact responses were not affected since they were measured only during the initial impact.

Since the impacter is assumed to remain in contact with the specimen throughout the impact event, the impacter displacement is used to give the displacement and velocity of the impacted face of the specimen. By assuming that frictional and heating effects are negligible, the energy imparted by the indenter is that absorbed by the specimen. Thus, this energy value at the end of the test is that irreversibly absorbed by the specimen.

The force data was post-processed with a low-pass discrete second order Butterworth filter to remove noise from the signal. Cut-off frequencies were selected to ensure no loss of pertinent features, and were also scaled as $1/s$ (as closely as possible) since time scales as s (Table 1). All data presented here is filtered for clarity, but the entire analysis was also duplicated using the raw data to confirm that the results were not affected by data filtering.

Each row in Table 1 corresponds to a series of tests on nominally identical specimens performed at a range of increasing incident velocities and hence energies. After testing, damage was observed and noted, and the projected area of internal delamination(s) could be measured using strong backlighting since the materials considered are translucent.

4. Results

Two coefficients of variation for the thickness are given in Table 1. The first is that of the average thickness of the specimens (from the four measurements on each specimen) and the second value (in parenthesis) is that between all measurements. The larger second value simply confirms that not only is there thickness variation between specimens, but also across the surface of each specimen itself. The CSM laminates are generally more variable, and also show an increase in this variability with thickness. This is thought to be due to greater instability of the wet CSM laminate as the agent bonding together the fibres dissolves in the resin.

The damage progression seen followed that detailed in previous work [27,28]. Circular internal delamination occurred at a very low incident energy for all tests. At higher energies, these delaminations grew and then fibre damage occurred. The thinner specimens tended to give ‘back-face fibre damage’ as large global deflections gave high strains. The thicker specimens tended to first give permanent indent damage on the ‘front’ or impacted face that then developed into ‘front-face fibre damage’. In both cases, once the initial damage became more severe with increasing energy, fibre damage could occur on the other face, leading to penetration, and finally perforation. ‘Fibre failure’ of the WR laminates consisted of breakage of the continuous fibres, whereas for CSM laminates ‘pull-out’ of the short discontinuous fibres occurred.

The force–displacement behaviour reflected the damage progression. The thicker WR and CSM response was as previously seen [27,28]; a bi-linear force–displacement response with a sudden reduction in stiffness as delamination occurred, and at higher impact energies a drop in force or an inflection due to fibre damage was evident.

The thinner WR tests for the test scales s = 1 and 2 exhibited the increasing stiffness and decreasing impact duration associated with membrane effects [27,28], but these were not present for the larger, s = 3 scale (see Section 5.3). Although delamination of the thinner WR specimens also occurred, no corresponding drop in stiffness was discernible [27,28].

The thinner CSM response also showed membrane stiffening effects for s = 1 and 2, but these were weaker than for the thinner WR, due to the lower diameter to thickness ratio of

the CSM specimens. Again these membrane effects were not present for the larger, *s* = 3 tests. However, for the thinner CSM specimens, a sudden drop in stiffness accompanied delamination.

The test results may be most clearly and concisely summarised graphically; the test variable of central deflection, and the other impact responses are plotted in Figs. 1–5. The appropriate scaling factors obtained in Section 2 are used to directly compare the responses at different scales. Section 2 also showed that scaling equivalence is obtained when the same incident velocity is used at each scale, and hence these responses are plotted against incident velocity. This also allows valid comparisons to be made when slight differences between nominal and obtained incident velocities occurred.

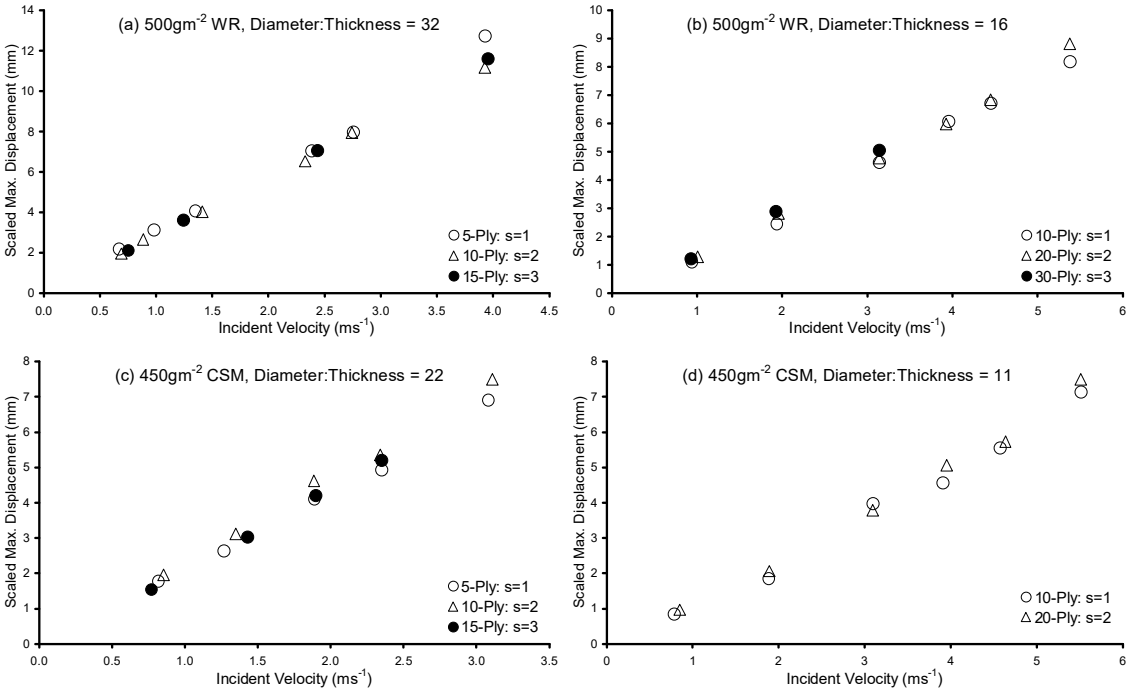

Fig. 1. Scaled maximum displacement results (scale factor *s*).

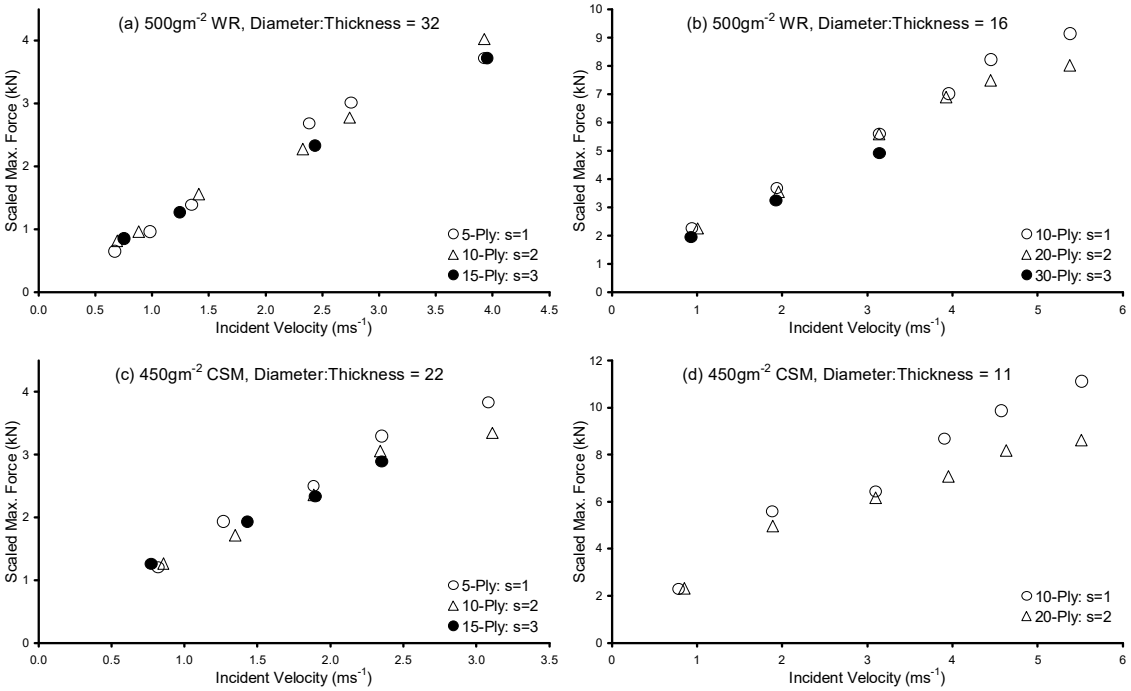

Fig. 2. Scaled maximum force results (scale factor s^2).

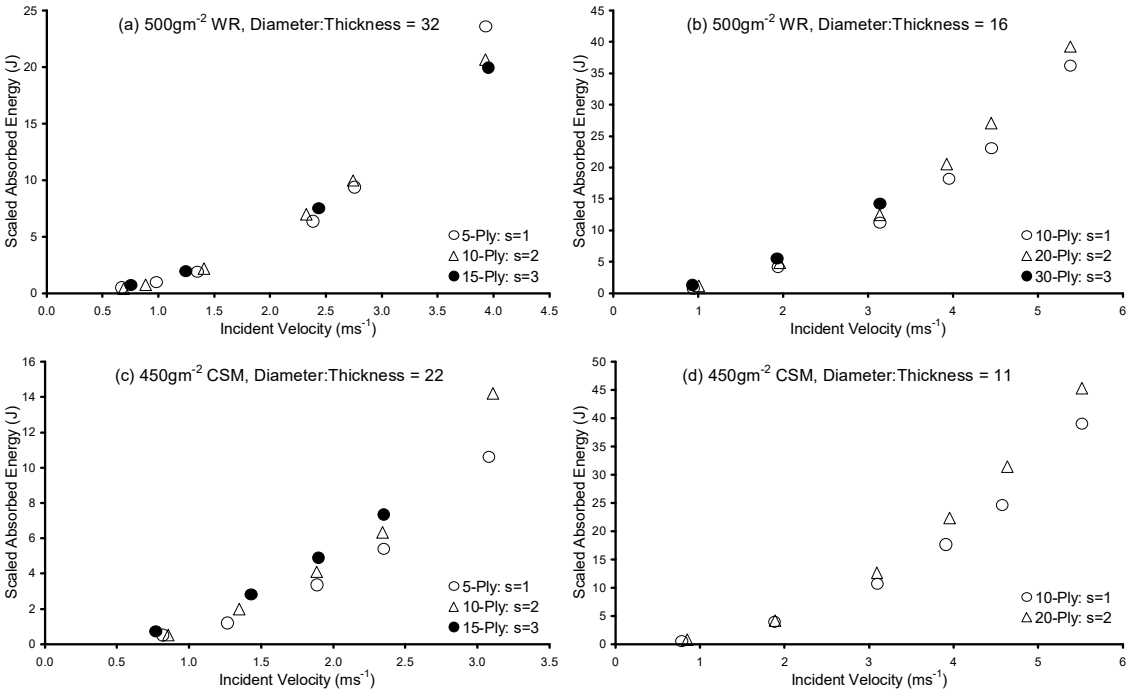

Fig. 3. Scaled (irreversibly) absorbed energy results (scale factor s^3).

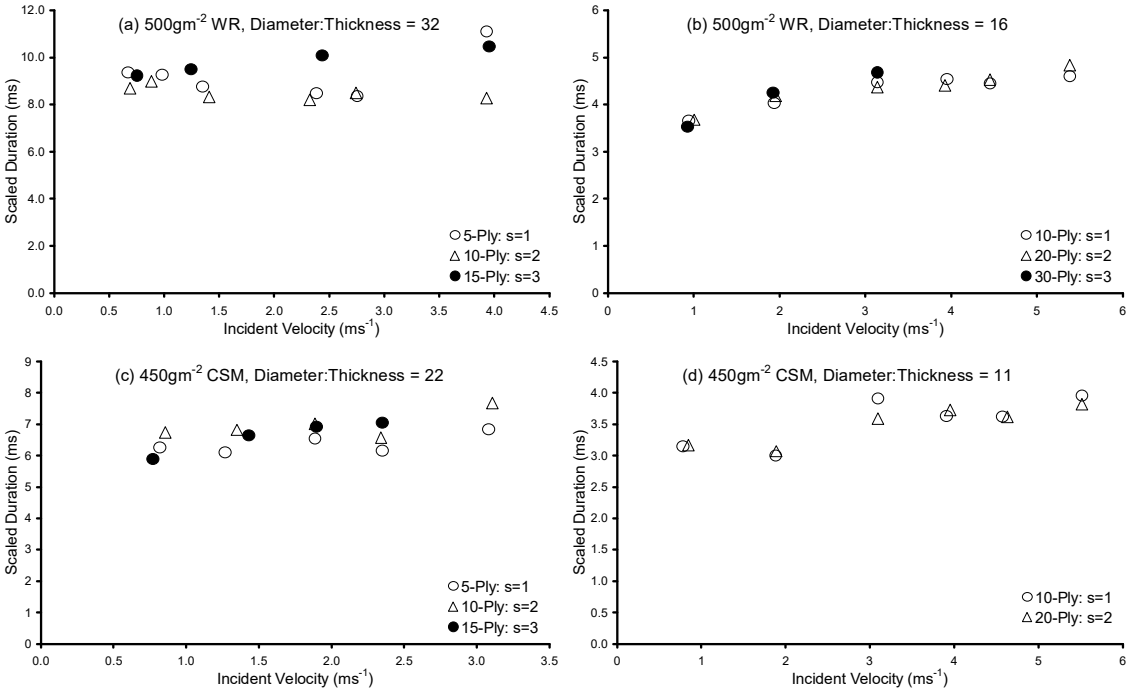

Fig. 4. Scaled impact duration results (scale factor *s*).

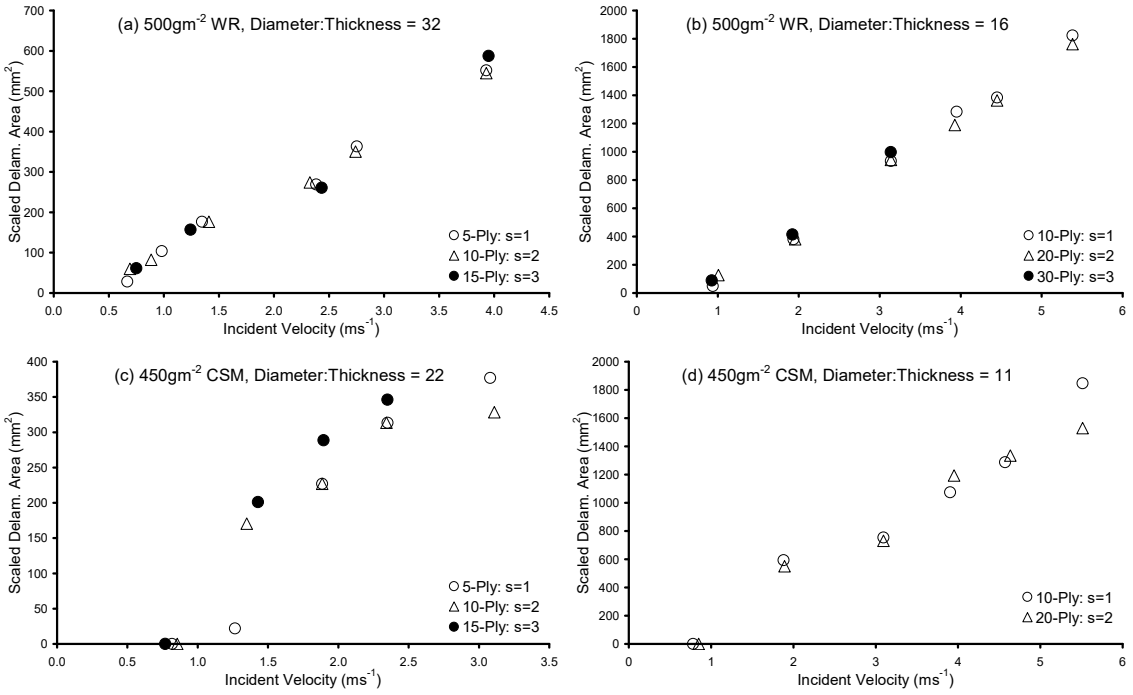

Fig. 5. Scaled delaminated projected area results (scale factor s^2).

5. Analysis and discussion of results

Most importantly, the scaling approach used here produced very accurate results despite the simplifying assumptions that the composite material is homogeneous and isotropic. Fig. 1 shows quite clearly that the central deflection has been scaled extremely

successfully. Figs. 2–5 show that the approach also scales very well the impact responses of maximum force, absorbed energy, impact duration and even projected delaminated area.

Interestingly, the analysis used here could equally apply to other boundary conditions (e.g., simply supported), suggesting that the same approach could also be successfully used for other cases. However, since impact damage modes are sensitive to changes in test set-up [29], this would have to be verified in each case experimentally.

However, there are some deviations from the analysis (i.e. 'size-' or 'scale effects') and these are discussed below.

5.1. Fibre damage

Fig. 2(b) and (d) show that at higher incident velocities the maximum force is lower for larger scale. This is accompanied by the higher absorbed energies for the larger scale at higher incident velocities shown in Fig. 3(b) and (d). This behaviour is due to the observation that fibre damage became more severe and occurred at lower incident velocities with increasing scale. The observed damage modes have been presented in Fig. 6, where the fraction of incident energy that is irreversibly absorbed is plotted against incident velocity.

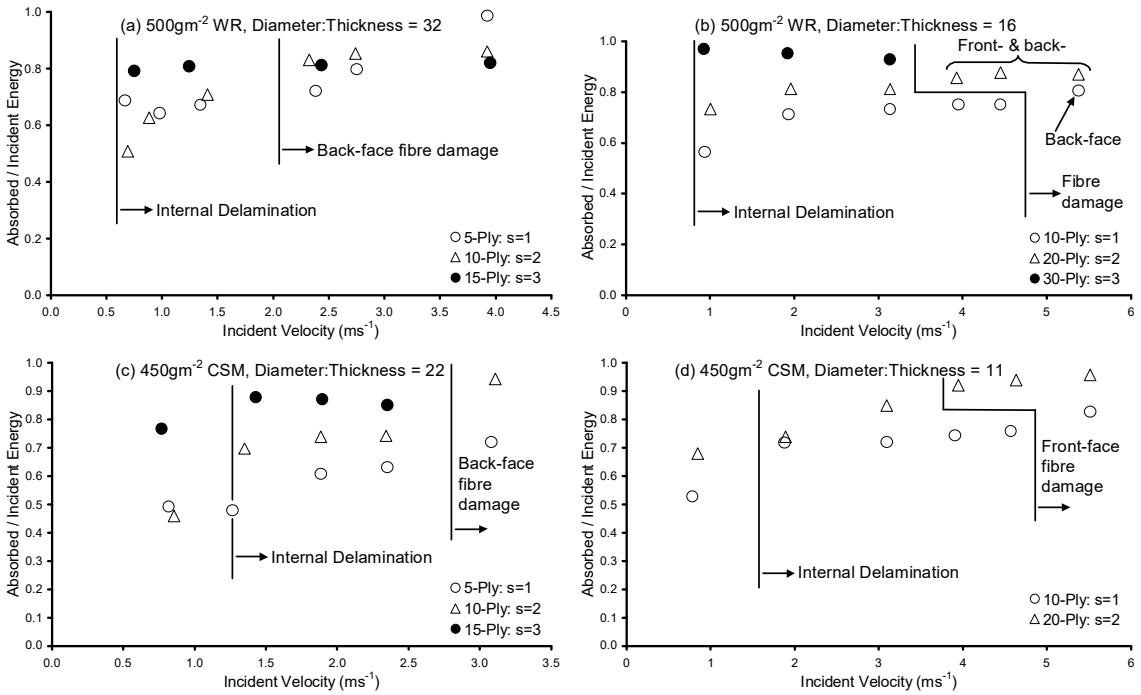

Fig. 6. Absorbed to incident energy ratio results.

The thicker WR and CSM specimens show clearly a fibre damage 'size effect'; damage is observed at a lower incident velocity for s = 2 than for s = 1. Furthermore, Fig. 7 shows the points (in terms of force–displacement) at which fibre damage initiated during the relevant tests. This figure clearly shows this onset of fibre damage size effect both not only for thicker specimens, but also for thinner specimens. Fig. 7 also shows that for the thinner WR specimens increasing the impact velocity delays fibre damage, i.e., some sort of strain-rate dependency is present.

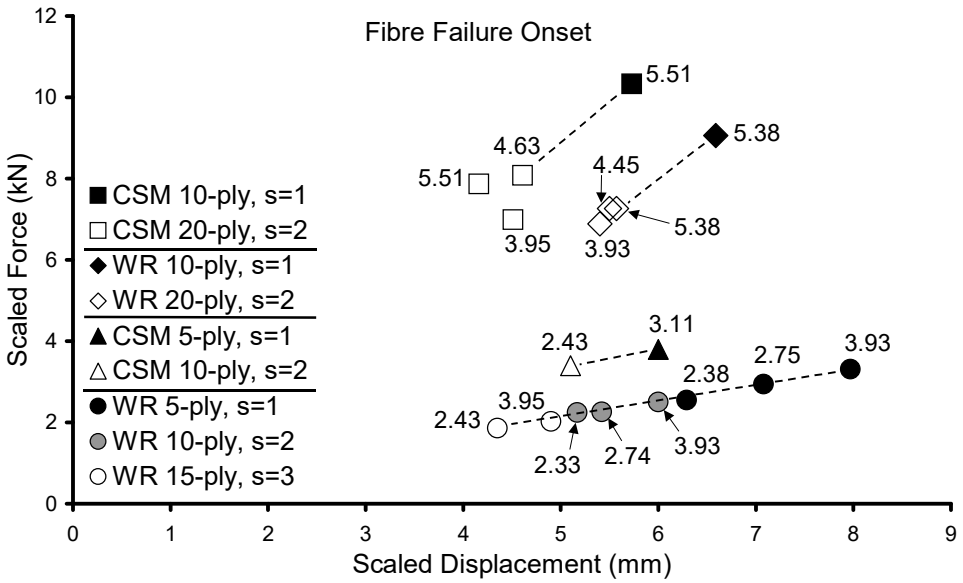

Fig. 7. First fibre failures (labels are incident velocities in ms^{-1}).

It is not clear what is responsible for this size effect, since the present experimental program was designed to give the overall impact behaviour and hence data concerning fibre damage is limited. Various theories have been postulated to explain composites strength size effects such as weakest link and Linear Elastic Fracture Mechanics theories [1,11]. Here, the complex damage modes that occur would further complicate any analyses, and there is even some evidence that failure modes may themselves vary with scale (Fig. 6(b)). It is also possible this observed 'size effect' could be inextricably linked with the 'strain rate' effect also seen, since when using the present modelling analysis as scale is increased the strain rate must decrease (i.e., $\lambda_t = s$).

Similarly, when considering the observed 'strain rate' effect, there is too little data to postulate explanations with confidence. However, the effect seen is large considering the very small changes in strain rate involved and hence the mechanism might well be more complex than that of the strain-rate dependency of the strength of composites [18,30], which is itself still not fully understood. Again it is relevant to point out that the damage mechanisms of impact on composites are complex and interacting.

Hence, we can only reasonably conclude that 'size' and 'strain rate' effects on initial fibre damage have been identified, and that further studies, specifically designed to investigate these effects, are required.

5.2. Absorbed energy

Closer inspection of Fig. 3 indicates that the trend of increasing absorbed energy with scale is also present, although not as strong, at lower incident velocities where no fibre damage occurs. In Fig. 6 the fraction of incident energy irreversibly absorbed is plotted to show more clearly that this absorbed energy 'size effect' is significant for all except the thinner WR specimens.

In Section 5.1 it was postulated that at higher velocities this effect is due to fibre damage, but what is (are) the responsible mechanism(s) at lower incident energies? An obvious

answer is that perhaps one (or more) of the other damage modes is also more severe at larger scales.

For thicker WR and CSM laminates the scaled displacements at which the impact force fell to zero showed a definite trend, increasing with scale. Since this is assumed to be the point at which the impactor head leaves the specimen surface this could indicate that there is relatively more permanent indentation for large scales.

Previous indentation work [31] has found the contact behaviour of these laminates to follow a Hertzian law [32] at lower contact forces, followed by a change to linear behaviour at a critical load, P_{crit} as significant contact damage occurs. For the Hertzian behaviour,

$$P = n\alpha^{3/2} \tag{17}$$

Where the contact stiffness, $n = \frac{4E^*\sqrt{R_i}}{3}$, $\frac{1}{E^*} = \frac{1-\nu_i^2}{E_i} + \frac{1-\nu^2}{E}$, and α is the indentation.

Hence, $$\alpha = \left(\frac{3P}{4E^*\sqrt{R_i}} \right)^{2/3} \tag{18}$$

i.e. $$\lambda_\alpha = s \tag{19}$$

That is the Hertzian indentation should scale geometrically, indicating no size effect. However, the previous work [31] showed the contact stiffness *n* not to be proportional to $\sqrt{R_i}$ as expected, and this departure from the theory could be a possible source of the absorbed energy size effect. The following expression was developed for P_{crit}

$$P_{crit} = \sqrt{\frac{6\,ILSS^3\pi^3h^3R_i}{E}} \tag{20}$$

i.e. $$\lambda_{Pcrit} = s^2 \tag{21}$$

which suggests that there should also be no size effect due to the transition to linear contact behaviour.

For the linear contact stiffness behaviour, the controlling mechanisms are not yet understood, and hence it is not possible to state whether this part of the indentation behaviour is responsible for any size effects or not. Similarly, little is known about the forms of the indentation 'unloading curves' (the response as the load falls), and so again this behaviour may or may not contribute to the observed absorbed energy size effect.

Even slight differences in the material itself could also affect the indentation behaviour between scales. For example, the degree of (hand) consolidation of the top layers could change with the number of unstable wet plies under them. Also, perhaps the fact that the reinforcement is not scaled could lead to differences in indent behaviour, for example due to the different relative sizes at each scale of the impactor head and the weave or chopped fibre dimensions.

Hence, indentation damage could contribute to the absorbed energy size effect, but the mechanisms are complex and not yet fully understood. However, Nettles et al. [12] found

that dent depths did not scale, and hence this suggests that contact damage could be at least partly responsible for this effect.

Delamination is another potential mechanism, but the delaminated areas scale very well suggesting that this failure mode does not absorb relatively more energy at larger scales. However, these values are only projected areas, the exact nature of the delaminations is more complex, and so it is still possible that delamination contributes in some way to the absorbed energy size effect.

Furthermore, previous work [27] found that even when no visible damage occurred, most of the incident energy was irreversibly absorbed. It is not yet known if this energy is absorbed by unseen damage such as matrix cracking, or by other mechanisms such as visco-elastic damping or friction. Hence, other unconsidered damage, or other, mechanisms could also be fully or partly responsible for this absorbed energy effect.

Again, given the data available and the number and complexity of possible explanations, we may only conclude that further study is required before we can try to clarify the observed scale dependency of absorbed energy.

5.3. Impact durations

In Fig. 4(a) the scaled impact durations of the WR s = 3 (15-ply) specimens increase with incident velocity, whilst those of the two smaller scales decrease due to membrane stiffening effects as noted in Section 4. A similar, but weaker trend is also visible in Fig. 4(c).

In order to further explore this we include bending, shear and membrane stiffness' k_b, k_s and k_m in the dimensional analysis;

$$\Pi_{14} = k_b / hE \text{, i.e. } \lambda_{kb} = s \quad (22)$$

$$\Pi_{15} = k_s / hE \text{, i.e. } \lambda_{ks} = s \quad (23)$$

$$\Pi_{16} = k_m h / E \text{, i.e. } \lambda_{km} = 1/s \quad (24)$$

This might appear to suggest that membrane effects should become less important with increasing scale.

However, $P = P_m + P_{bs} = k_{bs} w + k_m w^3$, (25)

Where $k_{bs} = \dfrac{k_b k_s}{k_b + k_s}$ giving $\lambda_{kbs} = s$, (26)

Hence, we can see that the 'stiffness' in terms of the variation of force with displacement scales as s^2 for both bending/shear and membrane stretching.

i.e. $\lambda_{Pbs} = \lambda_{Pm} = s^2$ (27)

That is, the scaled force–displacement plots and the relative effects of membrane and bending/shear on impact duration should not change with scale.

Another possibility is that, despite the efforts to scale the clamping system, the boundary conditions at the largest scale were not exactly equivalent to those at the smaller scales. Greater slippage of specimen between the clamps could be responsible, but through-bolting should have prevented this, and no damage to the holes in the larger specimens indicated that this had in fact occurred. However, it was not practicable to exactly scale the entire

clamping/support set-up and so relatively larger clamping/support deflections due to the much higher membrane forces at the largest scale are also still possible explanations.

Again this effect requires further investigation, but initial findings indicate that the exact scaling of the boundary conditions is extremely important.

6. Conclusions

A dimensional analysis approach has been used to develop scaling laws for impact on marine composite materials. An experimental study has been carried out to verify these relationships for the transverse impact of a hemispherical ended impactor on fully clamped circular plates at three different scales.

Although the model was a simplified one, the tests showed that it scaled the impact responses extremely well for the elastic response.

However, deviations from the predictions with scale, or 'size effects' were observed:

- The onset of fibre failure was found to be at a relatively lower load and displacement for larger scale specimens.
- For thinner woven roving specimens a higher strain rate also resulted in an earlier fibre failure.
- Relatively more energy was irreversibly absorbed for larger specimens even before fibre damage occurred.
- Membrane stiffening effects were weakest at the largest scale.

The mechanisms behind these effects have been discussed, and postulations made on the bases of the observations made, but further work is required, especially to investigate the scaling of fibre failure and how this relates to penetration and finally perforation.

Acknowledgements

This work has been performed within the project "MARSTRUCT – Network of Excellence on Marine Structures" (http://www.mar.ist.utl.pt/marstruct/) and has been partially funded by the European Union through the Growth programme under contract TNE3-CT-2003-506141. The first author is financed by the Portuguese Foundation of Science and Technology under the contract number SFRH/BPD/20547/2004.

References

[1] Abrate S. Impact on Composite Structures. Cambridge University Press, Cambridge UK, 1998.

[2] Wisnom MR. Size effects in the testing of fibre-composite materials. Composites Science and Technology 1999;59(13):1937-1957.

[3] Morton J. Scaling of impact-loaded carbon-fiber composites. AIAA Journal 1988;26(8):989-994.

[4] Pintado P and Morton J. On the scaling of impact loaded composite beams. Composite Structures 1994;27(4):357-365.

[5] Sutherland LS, Shenoi RA and Lewis SM. Size and scale effects in composites: I. Literature review. Composites Science and Technology 1998;59:209-220.

[6] Qian Y, Swanson SR, Nuismer RJ and Bucinell RB. An experimental study of scaling rules for impact damage in fiber composites. Journal of Composite Materials 1990;24(5):559-570.

[7] Swanson SR, Smith NL and Qian Y. Analytical and experimental strain response in impact of composite cylinders. Composite Structures 1991;18(2):95-108.

[8] Swanson SR. Mechanics of transverse impact in fiber composite plates and cylinders. Journal of Reinforced Plastics and Composites 1993;12:256-267.

[9] Swanson SR. Scaling of impact damage in fiber composites from laboratory specimens to structures. Composite Structures 1993;25(1-4):249-255.

[10] Sankar BV. Scaling of low-velocity impact for symmetric composite laminates. Journal of Reinforced Plastics and Composites 1992;11:297-305.

[11] Ambur DR, Prasad CB, Rose CA, Feraboli P and Jackson WC. Scaling the nonlinear impact response of flat and curved anisotropic composite plates. In: Proceedings of 46th AIAA/ASME/ASCE/AHS/ASC Structures, Dynamics and Materials Conference, Austin, TX, 2005.

[12] Nettles AT, Douglas MJ and Estes EE. Scaling effects in carbon/epoxy laminates under transverse quasi-static loading. NASA Technical Memorandum NASA/TM-1999-209103, 1999.

[13] Jackson KE and Fasanella EL. Impact testing and simulation of a crashworthy composite fuselage. In: Proceedings of American Helicopter Society 56th Annual Forum, Virginia Beach, Virginia, May 2-4, 2000.

[14] Found MS, Howard IC and Paran AP. Size effects in thin CFRP panels subjected to impact. Composite Structures 1997;38(1-4):599-607.

[15] Liu D, Raju BB and Dang X. Scaling effects on impact response of composite laminates. International Journal of Impact Engineering 1998;21(10):837-854.

[16] Robinson P and Davies GAO. Impactor mass and specimen geometry effects in low velocity impact of laminated composites. International Journal of Impact Engineering 1992;12(2):189-207.

[17] Davies GAO and Zhang X. Impact damage prediction in carbon composite structures. International Journal of Impact Engineering 1995;16(1):149-170.

[18] Zhou G and Davies GAO. Impact response of thick glass fibre reinforced polyester laminates. International Journal of Impact Engineering 1995;16(3):357-374.

[19] Kistler LS and Waas AM. Impact response of cylindrically curved laminates including a large deformation scaling study. International Journal of Impact Engineering 1998;21(1-2);61-75.

[20] Tomblin JS, Raju KS and Arosteguy G. Damage resistance and tolerance of composite sandwich panels- scaling effects. U.S. Department of Transportation, Federal Aviation Administration Report No. DOT/FAA/AR-03/75, 2004.

[21] Moody RC, Harris JS and Vizzini AJ. Scaling and curvature effects on the damage tolerance of impacted composite sandwich panels. Journal of Sandwich Structures and Materials 2002;4(1):71-82.

[22] Zenkert D, Shipsha A, Bull P and Hayman B. Damage tolerance assessment of composite sandwich panels with localised damage. Composites Science and Technology 2005;65(15-16):2597-2611.

[23] Chen VL, Wu HYT and Yeh HY. A parametric study of residual strength and stiffness for impact damaged composites. Composite Structures 1993;25(1-4):267-275.

[24] David FW, Nolle H. Experimental modelling in engineering. London: Butterworths, 1982.

[25] Langhaar HL. Dimensional analysis and theory of models. New York: Wiley, 1951.

[26] Taylor ES. Dimensional analysis for engineers. Oxford: Clarendon Press, 1974.

[27] Sutherland, LS and Guedes Soares C. Impact behaviour of typical marine composite laminates. Composites Part B: Engineering 2006;37(2-3):89-100.

[28] Sutherland LS and Guedes Soares C. Impact characterisation of low fibre-volume glass reinforced polyester circular laminated plates. International Journal of Impact Engineering 2005;31:1-23.

[29] Sutherland, LS and Guedes Soares C. The effects of test parameters on the impact response of glass reinforced plastic using an experimental design approach. Composites Science & Technology 2003;63:1-18.

[30] Zhou G, Davies GAO. Impact response of thick glass fibre reinforced polyester laminates. International Journal of Impact Engineering 1995;16(3):357-374.

[31] Hancox, NL. and Mayer RM. Design Data for Reinforced Plastics. London: Chapman and Hall, 1993.

[32] Sutherland LS, Guedes Soares C. Contact indentation of marine composites. Composite Structures 2005; 70(3):287–94.

[33] Johnson K.L. Contact mechanics. Cambridge: Cambridge University Press, 1985.